Research Article

Chemical Review and Letters
journal homepage: www.chemrevlett.com
ISSN (online): 2645-4947 (print) 2676-7279

A density functional theory study of adsorption dimethyl fumarate on the surface of the pristine of g-C_3N_4 and Fe, Ni and Cu decorated graphitic carbon nitride

Isaac Vaziri[1, *], Issa Amini[1], Mohammad Reza Poor Heravi[1], Rovnag Rzayov[2]

[1]*Department of Chemistry, Payame Noor University, Tehran, Iran*
[2]*Department of Engineering and Applied Sciences, Azerbaijan State University of Economics, UNEC, Azerbaijan*

ARTICLE INFO

Article history:
Received 25 April 2024
Received in revised form 19 June 2024
Accepted 21 June 2024
Available online 15 July 2024

Keywords:
Density functional theory,
sensor,
drug delivery system,
Graphitic Carbon Nitride,
Dimethyl Fumarate.

ABSTRACT

In this research, the possibility of sensing ability of dimethyl fumarate (DMF), by using pristine graphitic carbon nitride (g-C_3N_4) and decorated graphitic carbon nitride (g-C_3N_4) with Fe, Ni, and Cu have been systematically investigated and it has been attained desirable results. Adsorption characteristics of DMF on both pristine and decorated g-C3N4 have been calculated, utilizing Density Functional Theory (DFT) calculations. A comprehensive analysis of 28 complexes have performed in both gas and solvent phases to determine an effective sensor for DMF. Geometry optimizations and total energy calculations were executed, alongside a Density of States (DOS) analysis for the selected complexes, employing the B3LYP level of theory with the lanL2DZ basis set. The most robust interaction energy for the pristine g-C_3N_4-DMF complex (S1) was determined to be -10.86 Kcal.mol^{-1} in the gas phase, suggesting that the adsorption mechanism is of a physical nature. The suitable pristine g-C3N4-DMF complex in the solvent phase (S9) exhibited an adsorption energy of -6.59 Kcal mol^{-1}. Among the decorated complexes with Fe, S17 demonstrated the highest sensitivity, with a % ΔEg of -33.33%. Furthermore, for one of the Ni@ g-C_3N_4-DMF complexes, S22, the energy gap (Eg) significantly decreased from 0.79 to 0.60 eV (%ΔEg = -24.05%), underscoring the pronounced sensitivity of Ni@ g-C3N4 to DMF adsorption. Lastly, one of the Cu@ g-C_3N_4 complexes, S25, showed an Eads of -14.20 Kcal.mol-1 and a % ΔEg of -13.48%, indicating its potential as a suitable sensor and drug delivery system for dimethyl fumarate in the solvent phase.

1. Introduction

Multiple sclerosis (MS) is an inflammatory disease of the immune system that targets myelinated axons in the central nervous system (CNS), leading to varying levels of damage to both the myelin and the axons [1]. In multiple sclerosis (MS), key characteristics include inflammation, neurodegeneration, and gliosis. The presence of perivascular lymphocytic infiltration and macrophages leads to the destruction of the myelin sheaths that abnormally encase neurons [2,3]. Dimethyl fumarate (DMF) is an ester of fumaric acid that has been approved for the management of relapsing-remitting multiple sclerosis (RRMS). Its mechanism of action involves the succination of proteins, which results in the inactivation of proteins which are rich in cysteine [4]. Evidence derived from both clinical trials and real-world applications indicates that dimethyl fumarate serves as an effective therapeutic option for this patient demographic, with its advantages sustained over an extended period [5]. The extensive applications of this compound highlight the significance of understanding its environmental release, which poses a critical concern within various environmental media. Consequently, it is essential to identify effective methods for detecting this compound in natural settings.

In the last decade, a considerable number of researchers have directed their efforts toward

∗ Corresponding author; e-mail: mrheravi@yahoo.com
https://doi.org/10.22034/crl.2024.454286.1327

investigating the environmental consequences of pharmaceuticals that have accumulated in substantial quantities within ecosystems, uncovering concerning negative effects on various living organisms [6]. Various studies have indicated that over 60 different pharmaceuticals have been identified as contaminants in the soil and water across multiple countries [7,8]. The various forms of drug contamination present in the environment have both direct and indirect impacts on the health of humans, animals, and plants [9-12]. The release of pharmaceuticals in significant amounts into the environment necessitates the identification of their accumulation sites through the use of sensors. These sensors are essential for identifying the substances that are released, with Nano particles constituting a key category of these sensing technologies [13,14]. Nanostructures have received much attention as chemical sensors [15-18]. One of the newest Nano materials which has been studied and used in different area, is the graphitic Nano particle (NP) like Carbo nitride (g-C_3N_4). For example, in 2021Shamim et al [19] have investigated the possibility of delivery of cisplatin drug by g-C_3N_4. Their results showed that the Eads of carboplatin by g-C_3N_4 is higher in the gas phase (−1.39 eV) than in the aqueous phase (−0.52 eV). Thus, the carboplatin g-C_3N_4 system is more stale in gaseous environment than in the aqueous media. As another example, Jiang et al. in 2021, Research has indicated that nanocomposites based on g-C_3N_4 may serve as effective carriers for the delivery of cisplatin [20] and phosphorene drug [21]. Among the different allotropes of g-C3N4, including the α-phase, β-phase, and graphite-like structures, graphitic carbon nitride is regarded as the most stable allotrope [22,23]. Two structural models had been proposed for the g-C_3N_4, consisting of either triazine units or heptazine rings (tri-s-triazine), in which heptazine rings were predicted to be more energetically favored building-blocks of g-C_3N_4 structures [24]. Chou-Yi Hsu et al. in 2023, research has focused on the probability of delivering of three of the most important drugs for treatment of MS disease have been investigated by using the heteroatom-decorated g-C_3N_4 QDs (by phosphorus and arsenic atoms). Based on studies conducted on the adsorption process and calculated Eads and ΔEg, concluded that the of P-g-C_3N_4 QD could not be a good sensor for detection of each of the three considered drugs. Also, the results showed that compared to pristine and P-g-C_3N_4 QDs, the As- g-C_3N_4 QD is not a suitable candidate to be applied as a carrier for drug delivery (due to its relatively higher Eads at least in the cases of DMF (Eads = - 6.09 kcal mol-1), and DXF (Eads = - 0.14 kcal mol-1)). While, it would be an accurate semiconductor sensor for selective detection of each mentioned drug (by creating strong electronic signals) [25]. The relatively moderate level of bond gap of pristine g-C_3N_4 (about 2.7 eV) leads that to exhibit a good performance in sensing different types of chemical compounds like the bioactive ones [19]. Therefore, scientists began to modify the structure of the pristine form in order to find new derivatives with better properties. Heteroatom doping, surface functionalization, as well as changing the size or substrates are of the most practiced methods for improving such Nano structures [19-21].

On the other hand, have used the DFT approaches for modification of g-C_3N_4 respectively. Also, continues reports showed that the quantum mechanical methods give precious information about such structures [19,24]. In this manuscript, the sensing ability of pristine g-C_3N_4, Ni, Fe and Cu Decorated g-C_3N_4 were studied in identifying the DMF drug. The interaction of DMF with the pristine g-C_3N_4 and g-C_3N_4 decorated with the Ni, Fe and Cu was investigated to find the preferred adsorption sites, interaction energies and sensing ability using DFT calculations. The results of this research can be useful for making an adsorbent for the DMF drug and provide suitable sensing.

2. Calculation methods and structures

In this research, all computations were conducted utilizing the Density Functional Theory (DFT) approach at the B3LYP/lanL2DZ theoretical level, employing the Gauss view 06 and Gaussian 09 programs. The B3LYP method is the most widely utilized density functional in the research of nanostructured materials [26-28]. A review of the literature suggests that the B3LYP density functional is both appropriate and dependable for forecasting the structural, optical, electronic, and energetic characteristics of various nanostructures [29] [30-35]. The Density Functional Theory (DFT) approach stands as one of the most robust techniques in quantum mechanical computations. During the optimization phase, the target molecular configurations are refined to attain the lowest possible energy, while simultaneously calculating the energy levels of the specified systems [36]. In order to achieve the minimum energy configuration for the g-C_3N_4 -DMF complex, as opposed to merely identifying a local minimum, scans of the Potential Energy Surface (PES) were conducted with respect to different dihedral angles. The Density of States (DOS) plots were generated utilizing the Gauss sum method [37]. A sensor is a device that responds to a specific stimulus and produces a measurable electrical signal. If the energy gap and adsorption energy are deemed suitable, one can infer that the Nano particle under investigation is appropriate for the

intended sensor application. The adsorption energy (E_{ad}) is calculated as follows:

$$E_{ads} = E_{Compelex} - E_{g\text{-}C3N4} - E_{DMF} + E_{BSSE} \quad (1)$$

E(BSSE) is the Basis Set Superposition Error (BSSE) corrected for all adsorption energies using the counterpoise method [38]. In this study, some interaction indicators useful for the analysis were evaluated. Strong interactions are not favorable in drug sensing because of a long recovery time and thus hard desorption of a drug over a nanoparticle. With more negative Ead, the recovery time (τ) is increased and this may be determined using the following equation [39,40]:

$$\tau = \nu^{(-1)} \exp^{(-Ead/KT)} \quad (2)$$

Here τ is the recovery time and ν is the attempt frequency, T is the temperature, and K is the Boltzmann constant [41]. According to this equation, there is an exponential relationship between Eads and recovery time. The large recovery time is the main problem that can be solved by heating the sensor to a high temperature [42]. Vacuum-UV is applied for the recovery of drugs from the surface of the graphene system. The HOMO-LUMO gap is the difference between LUMO and HOMO that showed with Eg [43-54].

The energy gap (Eg) of the studied structures is computational calculated as follows:

$$E_g = E_{LUMO} - E_{HOMO} \quad (3)$$

When we evaluate the electronic sensitivity of the nanostructure to a drug, the HOMO and LUMO energy deformation are calculated as follows:

$$\%\Delta E_g = \left[\frac{\left(E_{g\ complex} - E_{g\ nano\ particle}\right)}{E_{g\ nano\ particle}}\right] \times 100 \quad (4)$$

The chemical potential of each system or the Fermi level (EFL), was obtained from equation:

$$E_F = \frac{-(E_{LUMO} + E_{HOMO})}{2} \quad (5)$$

Density Functional Theory (DFT) calculations revealed that the electronic characteristics of g-C_3N_4 were altered upon the adsorption of the drug molecule. The electronic sensitivity of the sensor may be evaluated subsequent to the alteration of the energy levels of the HOMO and LUMO orbitals of the complex in relation to the nanostructure. In order to answer the question of whether this Nano particle is a suitable sensor or not, it is necessary to examine two factors: adsorption energy and gap energy. By diminishing the energy of the gap, the proficiency to transmit the electrical signal is augmented. It was pointed out that E_g is proportional to the conduction electron population (σ) represented in Equation (6). σ increases as the energy gap (E_g) decreases with the adsorption of DMF on g-C3N4. On the other hand, when $-\%\Delta E_g$ increases, the potential detection also increases. The correlation between E_g and the electrical conductivity of nanostructures is as follows:

$$\sigma = AT^{\frac{3}{2}} \exp(-Eg/KT2) \quad (6)$$

Where K is Boltzmann's constant and A (electrons/$m^3K^{3/2}$) is a constant. There is an acceptable correlation between the results obtained by this method and experimental techniques [55]. Equation (6) is used to study the sensitivity of a nanostructure to a drug. This allows electrical conductivity to be converted into an electrical signal associated with the presence of drug molecules [56,57].

3. Results and Discussion

Continuing previous work on the various areas of organic compounds, in this work, the adsorption of Dimethyl fumarate on the surface of the pristine, Fe, Ni, and Cu-decorated g-C_3N_4 was investigated.

3.1. The pristine g-C_3N_4 Characterization

The pristine, Ni, Fe and Cu-decorated g-C_3N_4 QDs were separately designed as input files, and were then optimized step by step to the B3LYP/lanL2DZ level of theory (to give the more stable geometries). In addition, the related parameters were extracted from the output files and the obtained information in the gaseous and solvent phases for pristine state are listed in Table 1. The optimized structures of g-C3N4 are shown in Figure 1. The pristine g-C_3N_4 consists of 18 C, 9 H and 27 N atoms and the ends of the atoms are saturated with 9 hydrogen atoms.

The presence of hydrogen atom in two-dimensional crystalline and amorphous carbon nitride structure has been investigated [58]. The calculated structural energy for g-C_3N_4 at the B3LYP/lanl2dz theoretical level is measured at -59.02 KeV, signifying the considerable stability associated with this molecular configuration.

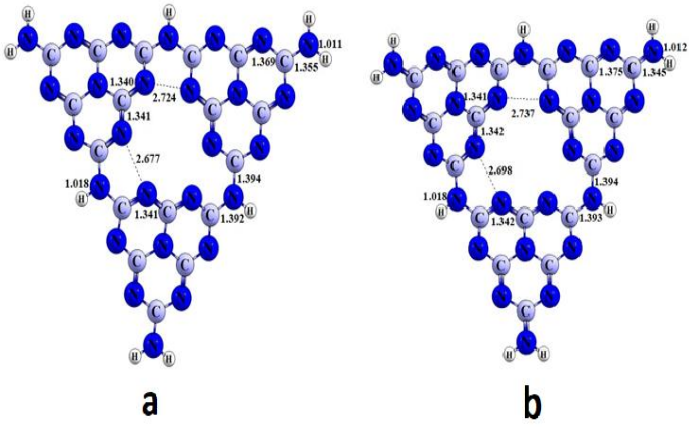

Fig. 1. Optimized structure of g-C_3N_4 in (a) gas and (b) solvent phases.

The binding energy (E_b) was determined through the subsequent equation to demonstrate the stability of the pristine state:

$$E_b = \frac{[E_{Pristine} - (18E_C + 27E_N + 9E_H)]}{54} \qquad (7)$$

This Nano particle constitutes a stable substance as evidenced by the calculated binding energy of -10.13 eV. The HOMO energy of g-C_3N_4 in gas phase is approximately -6.47 eV and the LUMO energy is -3.00 eV Thus, the E_g is nearly 3.47eV (Table 1). Through the transition of the phase from gaseous to aqueous solvent, there has been reduction in the energy levels of the HOMO and LUMO, consequently leading to decrease in the energy of the Fermi level. Furthermore, an augmentation in the energy gap has been observed. Total Density of States (TDOS) diagrams pertaining to the pristine of g-C_3N_4 in gas and solvent phases are illustrated in Figure2. It is evident from the diagram that the energy level of the band gap has risen from 3.47 eV in the gaseous phase to 3.64 eV in the solvent phase.

3.2. The Dimethyl Fumarate Characterization

The optimized structure of dimethyl fumarate at the B3LYP/lanl2dz theoretical level is shown in Figure 3. To confirm the actual minimization of energy, frequency calculations (FREQ=NORAMAN) were performed and all frequencies obtained were positive. The calculated structural energy is equal to -14.53 KeV and other information related to the structural energies of this drug is recorded in Table 2.

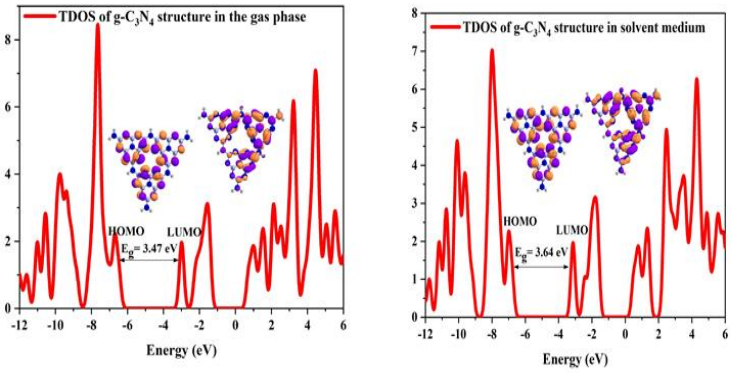

Fig. 2. Total Density of States of g-C3N4 structure in gas and solvent phases.

3.3. The adsorption of DMF on the g-C_3N_4 in gas phase

In order to identify a stable structure, it is imperative to conduct optimization calculations. Within the framework of the optimization methodology, the molecules undergo optimization utilizing a suitable technique for the computation of interatomic forces, thereby facilitating the rearrangement of molecules to achieve the maximum adsorption energy. To ascertain the stable configurations (global minima) of an DMF pharmaceutical adsorbed onto g-C_3N_4, a variety of studies have been executed. Ultimately, two active sites of the drug are anticipated, encompassing the oxygen within the carbonyl group (C=O) and the oxygen atom in the ester functional group (-COO-), which allows the drug to adsorb onto the hydrogen atom that is covalently bonded to the nitrogen atom of g-C_3N_4 (hydrogen bond formation). As depicted in Figure 4, total of eight distinct complexes were identified, illustrating the interactions between the active sites of dimethyl fumarate (DMF) and g-C_3N_4. The equilibrium distances between the drug molecule and the surface of the Nano particle in the eight investigated structures are as follows:

S6 > S8 > S7 > S5 > S3 > S1 > S2 > S4

As indicated in Table 2, the HOMO energy level transitioned from -6.47 eV in pristine g-C_3N_4 to -6.43 eV in the most stable complex which is named S1, representing a shift towards higher energy levels. Conversely, the LUMO energy level changed from -3.00 eV to -3.06 eV, reflecting a shift towards lower energy. Nevertheless, these alterations did not influence the Fermi level energy, which remained constant at -4.74 eV for the S1. In S1, the drug was observed to be adsorbed from the oxygen within the carbonyl functional group onto g-C_3N_4 at a distance of 1.808 Å. The computed %ΔEg for all complexes (except S3) exhibit negative characteristics.

Nevertheless, the frequency of these alterations is minimal, rendering them unsuitable for sensory applications. According to Table 3, there is an observable slight alteration in the energy states of the HOMO and the LUMO complexes as the drug molecule transitions toward the nanoscale dimensions. these changes have led to a decrease in E_g in all complexes (except S3). Consequently, all alterations in the values of energy gap variations are characterized by negativity, with the most significant modifications, quantified at -3.86%, being associated with the S1 complex. Among the analyzed structures, the configuration denoted as S1 is characterized by the lowest adsorption energy, quantified at -10.86 kcal/mol. Consequently, this particular structure represents the most thermodynamically favorable adsorption configuration in the gaseous phase. This finding aligns with the observation that the length between the drug and the pristine surface in S1 constitutes one of the shortest equilibrium distances. The outcomes derived from the computations indicate that the Absolute value of the energy disparity between the HOMO of pristine of g-C_3N_4 and the LUMO of dimethyl fumarate (3.54 electron volts) is less than the Absolute value of the energy disparity between the HOMO of dimethyl fumarate and the LUMO of the pristine of g-C_3N_4 (4.77 electron volts), thus establishing the directionality of electron transfer from the HOMO of the pristine of g-C_3N_4 to the LUMO of the pharmaceutical agent dimethyl fumarate. The negation of the natural bond orbital (NBO) charges associated with the carbon and oxygen atoms within the drug molecule further corroborates this electron transference.

3.4. Pristine of g-C_3N_4 – DMF Complex in solvent phase

The outcomes derived from the computations indicate that the absolute value of the energy disparity between the HOMO of pristine of g-C_3N_4 and the LUMO of dimethyl fumarate (3.54 electron volts) is less than the absolute value of the energy disparity between the HOMO of dimethyl fumarate and the LUMO of the pristine of g-C_3N_4 (4.77 electron volts), thus establishing the directionality of electron transfer from the HOMO of the pristine of g-C_3N_4 to the LUMO of the pharmaceutical agent dimethyl fumarate. The negation of the natural bond orbital (NBO) charges associated with the carbon and oxygen atoms within the drug molecule further corroborates this electron transference. Among these 8 configurations, once more, the minimal equilibrium distance between the pharmaceutical agent and the nano particle is associated with the interaction between the carbonyl oxygen of the DMF molecule and the hydrogen atom bonded to the nitrogen in the g-C_3N_4 (hydrogen bond), which is observed in the S9 configuration and its length is 1.765 Å. The hierarchy of equilibrium distance from the greatest to the least are as follows:

S16 > S15 > S14 > S13 > S12=S11 > S10 > S9

Table 4 shows only slight variations in gap energy, and when considered alongside equation 6, this implies that the Nano particles' sensitivity as a drug sensor was restricted. Negative Eads values suggest that the adsorption process is feasible. The adsorption energy values vary depending on the specific adsorption configurations and sites examined. Among the analyzed structures, S9 exhibits the lowest adsorption energy at -6.59 kcal.mol^{-1}, indicating it represents the most favorable adsorption configuration in the solvent phase. This finding aligns with the observation that the distance between the drug and the pristine surface in S9 is the shortest equilibrium distance. The results indicate that, in the solution state, all adsorption interactions are characterized as physical and weak, as evidenced by the measured gap energies, adsorption energies and equilibrium distances, which contribute to a reduction in retention time.

3.5. The decorated g-C_3N_4 Characterization in gas phase

The decorated of transition metals within the pristine structural of g-C_3N_4 results in an elevation of the HOMO energy, accompanied by a reduction in the LUMO energy. Consequently, these alterations have precipitated a significant diminution in the gap energy of the decorated g-C_3N_4, suggesting an enhancement in the electrical conductivity of the g-C_3N_4. The minimum gap energy is observed in Cu@g-C_3N_4, registered at 0.69 eV. An elevation in the Fermi level energy, coupled with a reduction in the work function, yields an augmentation in the current density for the decorated carbon nitrides. Figure 6 shows the optimized structures of decorated g-C_3N_4 structure and Table 5 indicate the calculated information related to decorated g-C_3N_4. In this research, the surface of g-C_3N_4 Nano particles is decorated with Fe, Cu, and Ni atoms, and the corresponding calculations have been conducted. In the examination of DMF-g-C_3N_4 complexes in the gaseous phase, structure S1 demonstrated the most effective adsorption characteristics, which are utilized in this part of research (S18, S20, and S21). Furthermore, the interaction between the drug and the g-C_3N_4surface has been analyzed in scenarios where the drug is positioned above the metallic

Table 1. Energy of HOMO and LUMO, energy difference of HOMO and LUMO (E_g), Fermi level energy (EFL), work function (Φ) for pristine of g-C_3N_4 in gas and solvent phase.

Systems	E_{HOMO} (eV)	E_{FL} (eV)	E_{LUMO} (eV)	E_g (eV)	Φ (eV)
g-C_3N_4 in gas phase	-6.47	-4.74	-3.00	3.47	4.74
g-C_3N_4 in solvent phase	-6.79	-4.97	-3.15	3.64	4.97

Table 2. Energy of HOMO and LUMO, energy difference of HOMO and LUMO (E_g), Fermi level energy (EFL), work function (Φ) for DMF.

Systems	E_{HOMO} (eV)	E_{FL} (eV)	E_{LUMO} (eV)	E_g (eV)	Φ (eV)
g-C_3N_4 in gas phase	- 7.77	-5.31	-2.86	4.91	5.31

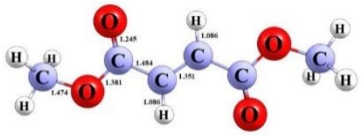

Fig .3. Optimized structure of DMF.

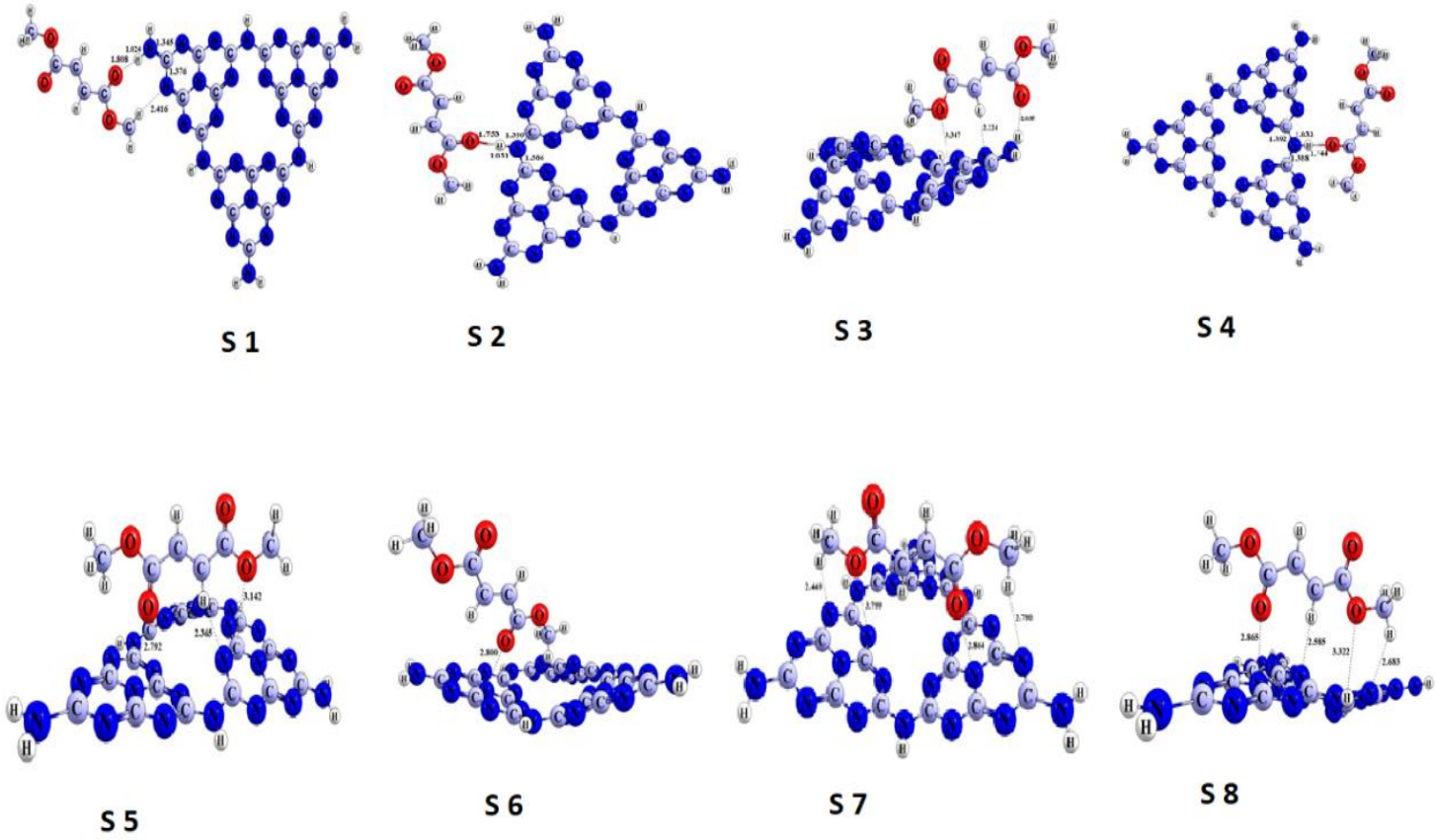

Fig. 4. . Optimized structures of DMF-g-C_3N_4 complexes in gas phase. Distances are in A.

Table 3. Adsorption energy (Eads), Energy of HOMO and LUMO, energy difference of HOMO and LUMO (Eg), Fermi level energy (EFL), the change of energy gap of g-C_3N_4 after adsorption (%ΔEg), work function (Φ), the change of work function of g-C_3N_4 after adsorption (ΔΦ), and Charge transfer between DMF molecule and g-C_3N_4 (QT). S1-S8 configurations at the theoretical level of B3LYP/ lanl2dz in the gas phase.

Systems	E_{ads} (kcal/mol)	E_{HOMO} (eV)	E_{FL} (eV)	E_{LUMO} (eV)	E_g (eV)	%ΔE_g	Φ (eV)	ΔΦ (eV)	Q_T (me)
g-C_3N_4	-	-6.47	-4.74	-3.00	3.47	-	4.74	-	-
S1	-10.86	-6.43	-4.74	-3.06	3.37	-3.86	4.74	0	23
S2	-10.09	-6.36	-4.64	-2.92	3.44	-1.75	4.64	-0.10	28
S3	-9.28	-6.49	-4.74	-2.99	3.50	1.10	4.74	0	3
S4	-9.14	-6.36	-4.64	-2.92	3.44	-1.75	4.64	-0.10	3
S5	-8.80	-6.40	-4.65	-2.90	3.50	-1.10	4.65	-0.09	1
S6	-8.78	-6.40	-4.71	-3.02	3.38	-3.63	4.71	-0.03	1
S7	-7.66	-6.38	-4.66	-2.95	3.43	-2.04	4.66	-0.08	1
S8	-6.55	-6.36	-4.63	-2.90	3.46	-1.25	4.63	-0.11	2

Table 4. Adsorption energy (Eads), Energy of HOMO and LUMO, energy difference of HOMO and LUMO (Eg), Fermi level energy (EFL), the change of energy gap of g-C_3N_4 after adsorption (%ΔEg), work function (Φ), the change of work function g-C_3N_4 after adsorption (ΔΦ), and Charge transfer between DMF molecule and g-C3N4 (QT) g-C_3N_4 structure. S9-S16 configurations at the theoretical level of B3LYP/ lanl2dz in the solvent phase.

Systems	E_{ads} (kcal/mol)	E_{HOMO} (eV)	E_{FL} (eV)	E_{LUMO} (eV)	E_g (eV)	%ΔE_g	Φ (eV)	ΔΦ (eV)	Q_T (me)
g-C_3N_4	-	-6.79	-4.97	-3.15	3.64	-	4.97	-	-
S9	-6.59	-6.76	-4.94	-3.12	3.64	0	4.94	-0.03	34
S10	-5.90	-6.77	-4.94	-3.11	3.66	0.55	4.94	-0.03	27
S11	-5.76	-6.75	-4.93	-3.12	3.63	-0.27	4.93	-0.04	27
S12	-5.68	-6.77	-4.95	-3.13	3.64	0	4.95	-0.02	26
S13	-3.51	-6.75	-4.92	-3.09	3.66	0.55	4.92	-0.05	2
S14	-3.13	-6.76	-4.93	-3.10	3.66	0.55	4.93	-0.04	4
S15	-2.98	-6.76	-4.94	-3.13	3.63	-0.27	4.94	-0.03	4
S16	-2.15	-6.75	-4.94	-3.13	3.62	-0.55	4.94	-0.03	2

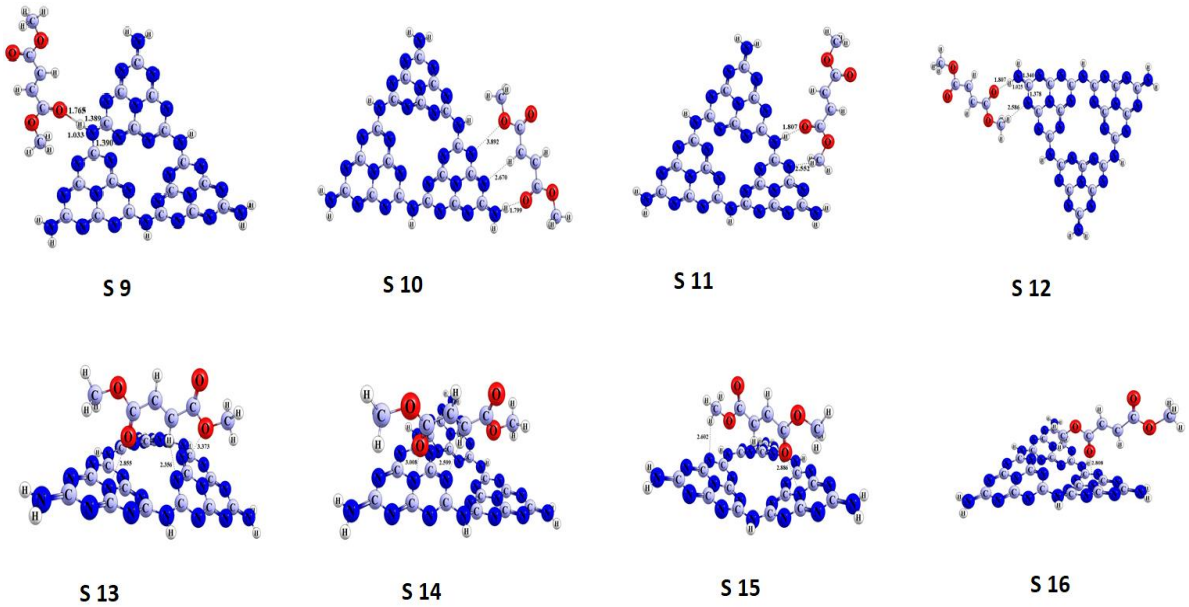

Fig. 5. Optimized structures of DMF- g-C_3N_4 complexes in solvent phase. Distances are in angstrom.

atom of the g-C_3N_4 structure (S17, S19 and S22). Table 5 presents the data obtained from the six analyzed structures of DMF- g-C_3N_4 complexes, as illustrated in Figure 7.

The configurations of S18, S20, and S21 complexes are analogous to the configuration of S1 complex, and the equilibrium distances of the pharmaceutical agent and Nano particle in these configurations are 1.717, 1.796, and 1.738 Å, respectively. Meanwhile, the equilibrium distance in the S1 configuration is equivalent to 1.808 Å. In all six complexes formed by the interaction of the DMF molecule with the decorated g-C_3N_4, there is a notable increase in the energy level of the LUMO, with the most significant changes observed in the S17, S21, and S22 complexes. The variations in the energy levels of the HOMO and LUMO for these complexes are illustrated in Fig.8. Except for the S20 complex, the energy gap is diminished when compared to the corresponding decorated g-C_3N_4 and the S17 structure exhibiting the smallest energy gap. The ranking of the energy gaps among these complexes is as follows:

S18 > S20 > S21 > S22 > S19 > S17

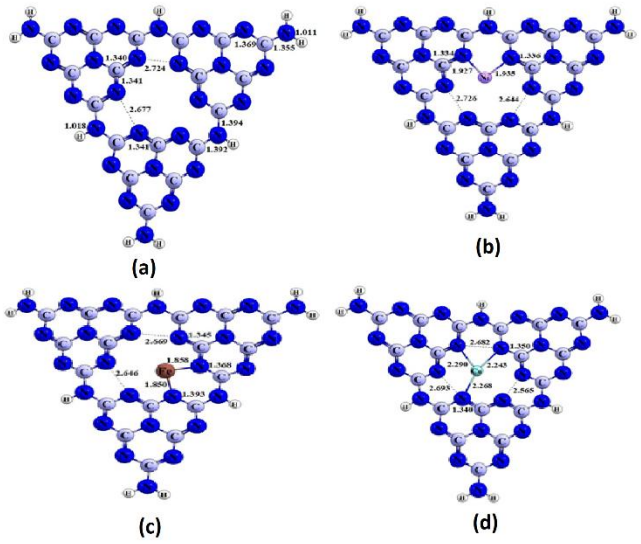

Fig. 6. Optimized structures of (a) g-C_3N_4 (b) Ni@ g-C_3N_4 (c) Fe@g-C_3N_4 (d) Cu@g-C_3N_4 in gas phase.

A reduction in the gap energy of the complex results in a negative the change of energy gap (%ΔEg), which correlates with an enhanced capacity for conducting electrical signals. A more pronounced negative value indicates a greater potential for the Nano particle to serve as an effective sensor candidate. The S17 structure exhibits the most significant alteration in gap energy, recorded at -33% for the change of energy gap. The trend of increasing %ΔEg from structures S17 to S22 are as follows:

S20 > S18 > S21 > S19 > S22 > S17

The decoration of Nano particles with Fe, Cu, and Ni metals results in a significant increase in the Fermi energy level. The energy values for the decorated Nano particles are measured at -3.50, -3.51, and -3.49, respectively, indicating that these values are quite close to each other. The modifications in the work function associated with the charge transfer between the decorated g-C_3N_4 and the DMF were determined using the following equation:

$$\Phi = E_{inf} - E_{FL} \qquad (8)$$

The electrostatic potential at infinity is denoted as Einf, while EFL represents the energy of the Fermi level. In this context, it is assumed that the electrostatic potential at infinity is equal to zero. Generally, a decrease in the work function can facilitate the emission of electrons from the surface of the semiconductor when an electric field is applied. The variations in the work function can be derived from the subsequent equation:

$$\Delta\Phi = \Phi\, complex - \Phi\, \text{nano} \qquad (9)$$

According to the calculations presented in Table 5 The most value the change in the work function is associated with the S17 structure, which exhibits a value of -0.15 eV. The positive value of the charge transfer factor (QT) indicates the movement of electric charge from the surface of the decorated g-C_3N_4 to the surface of the DMF. With the exception of the S17 complex, where a transfer of charge from the drug to the Fe@g-C_3N_4 has been observed, resulting in a negative charge transfer value, all other structures exhibited positive. In all of these complexes, the values of adsorption energy are negative, signifying that the adsorption process is both exothermic and thermodynamically favorable. The S17 complex exhibits the lowest adsorption energy at -18.32 kcal/mol. Additionally, the adsorption energy values for the S18 and S21 structures indicate a strong tendency for physical adsorption. The selection of sensors and drug carriers is significantly influenced by adsorption energy and gap energy. Among the Fe@g-C_3N_4 complexes of the S17 structure, the Cu@ g-C_3N_4 complexes of the S19 structure and the Ni@g-C_3N_4 complexes of the S21 structure exhibit more favorable and optimal conditions. Figure 9 illustrates the density of states plot for these three complexes.

3.5. The decorated g-C_3N_4 Characterization in solvent phase.

The decoration of Fe, Cu, and Ni metals into the g-C_3N_4 in a solvent phase resulted in an elevation of the HOMO energy and a reduction of the LUMO energy. These modifications led to a significant decrease in the energy gap of the g-C_3N_4, suggesting an enhancement in the electrical conductivity of the Nano particles. The energy band gaps for the various decorated g-C_3N_4 configurations are ranked as follows:

$$Fe@\ g\text{-}C_3N_4 > Cu@\ g\text{-}C_3N_4 > Ni@\ g\text{-}C_3N_4$$

Notably, the lowest energy gap was observed in Ni@ g-C_3N_4, measuring 0.78 electron volts. Additionally, the increase in fermi level energy and the decrease in work function contributed to a rise in the current density for all of the decorated g-C_3N_4 and Ni@ g-C_3N_4 exhibiting the lowest work function at 3.46 electron volts. Figure 10 illustrates the optimized structure of the g-C_3N_4 alongside the density of states diagram in the solvent state. Furthermore, Table 7 presents the calculated data for these complexes. A comparison of decorated g-C_3N_4 in solvent conditions versus gaseous conditions reveals that both the energy gap and the work function are elevated in solvent conditions relative to their gaseous counterparts. In order to examine the adsorption behavior of the dimethyl fumarate molecule on the surface of decorated g-C_3N_4 modified with Fe, Cu, and Ni metals in the solvent phase, the same structural configurations that were analyzed in the gas phase have been utilized. The structures of the S24, S26 and S27 complexes exhibit similarities to those of S1 and S9. Although in the S23, S25, and S28 complexes, the drug molecule is situated on the nanoparticle's surface. The optimized configurations of these six complexes, along with the data derived from their calculations, are presented in Figure 11 and Table 8. the equilibrium distances between the DMF and decorated g-C_3N_4 in the S26, S24, and S27 complexes has measured 1.798, 1.781, and 1.789 Å, respectively. In contrast, the equilibrium distance observed in the S1 configuration is recorded at 1.808 Å. As the drug molecule nears the nanoparticle's surface, alterations in the energy levels of the HOMO and the LUMO have been noted. A modest increase in the HOMO energy level has been recorded for all complexes, with the exception of the S23 structure, while a decrease in the LUMO energy level is observed across all complexes. In the solvent state, the energy gap for all complexes have founded to be lower than that of the decorated g-C_3N_4 gap energy, with the exceptions of the S23 and S26 structures. The S27 structure exhibits the lowest measured gap energy at 0.73eV.

Table 5 - Energy of HOMO and LUMO orbitals, energy difference of HOMO and LUMO orbitals (Eg), Fermi level energy (EFL), work function (Φ) for decorated g-C3N4 in gas phase.

Systems	E_{HOMO} (eV)	E_{FL} (eV)	E_{LUMO} (eV)	E_g (eV)	Φ (eV)
g-C_3N_4	-6.47	-4.74	-3.00	3.47	4.74
Fe@g-C_3N_4	-3.92	-3.50	-3.08	0.84	3.50
Cu@g-C_3N_4	-3.86	-3.51	-3.17	0.69	3.51
Ni@g-C_3N_4	-3.89	-3.49	-3.10	0.79	3.49

Table 6 - Adsorption energy (E_{ads}), Energy of HOMO and LUMO, energy difference of HOMO and LUMO (E_g), Fermi level energy (E_{FL}), the change of energy gap of g-C_3N_4after adsorption (%ΔE_g), work function (Φ), the change of work function of g-C_3N_4 after adsorption (ΔΦ), and Charge transfer between DMF molecule and decorated g-C_3N_4 in the gas phase.

Systems	E_{ads} (kcal/mol)	E_{HOMO} (eV)	E_{FL} (eV)	E_{LUMO} (eV)	E_g (eV)	%ΔE_g	Φ (eV)	ΔΦ (eV)	Q_T (me)
Fe@g-C_3N_4	-	-3.92	-3.50	-3.08	0.84	-	3.50	-	-
S17	-18.32	-3.63	-3.35	-3.07	0.56	-33.33	3.35	-0.15	-126
S18	-10.53	-3.83	-3.41	-3.00	0.83	-1.19	3.41	-0.09	30
Cu@g-C_3N_4	-	-3.86	-3.51	-3.17	0.69	-	3.51	-	-
S19	-7.67	-3.81	-3.52	-3.23	0.58	-15.94	3.52	0.01	523
S20	-1.48	-3.80	-3.42	-3.04	0.76	10.14	3.42	-0.09	25
Ni@g-C_3N_4	-	-3.89	-3.49	-3.10	0.79	-	3.49	-	-
S21	-10.24	-3.72	-3.38	-3.04	0.68	-13.92	3.38	-0.11	28
S22	-7.42	-3.71	-3.41	-3.11	0.60	-24.05	3.41	-0.08	14

Table 7. Energy of HOMO and LUMO orbitals, energy difference of HOMO and LUMO orbitals (Eg), Fermi level energy (E_{FL}), work function (Φ) for decorated g-C_3N_4 in the solvent phase.

Systems	E_{HOMO} (eV)	E_{FL} (eV)	E_{LUMO} (eV)	E_g (eV)	Φ (eV)
g-C_3N_4	**-6.79**	**-4.97**	**-3.15**	**3.64**	**4.97**
Fe@g-C_3N_4	**-4.25**	**-3.63**	**-3.01**	**1.24**	**3.63**
Cu@g-C_3N_4	**-3.98**	**-3.53**	**-3.09**	**0.89**	**3.53**
Ni@g-C_3N_4	**-3.85**	**-3.46**	**-3.07**	**0.78**	**3.46**

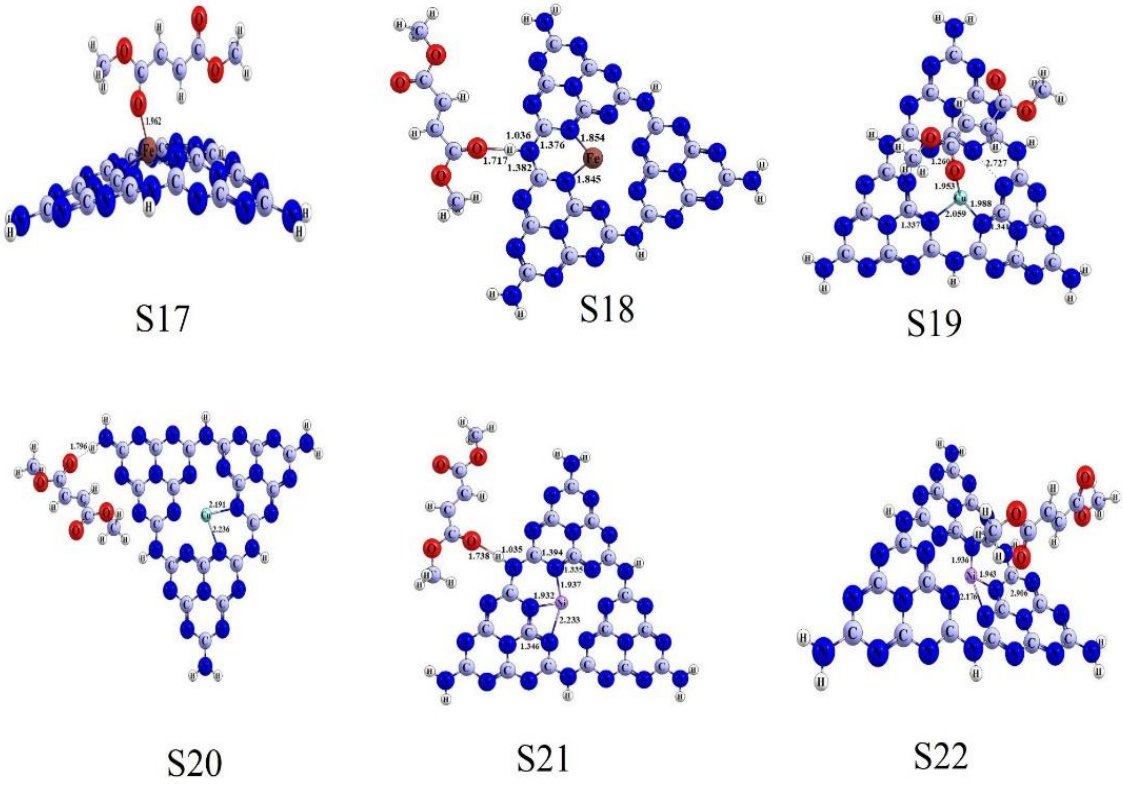

Fig. 7. Optimized structures of DMF- decorated g-C_3N_4 complexes in gas phase. Distances are in A.

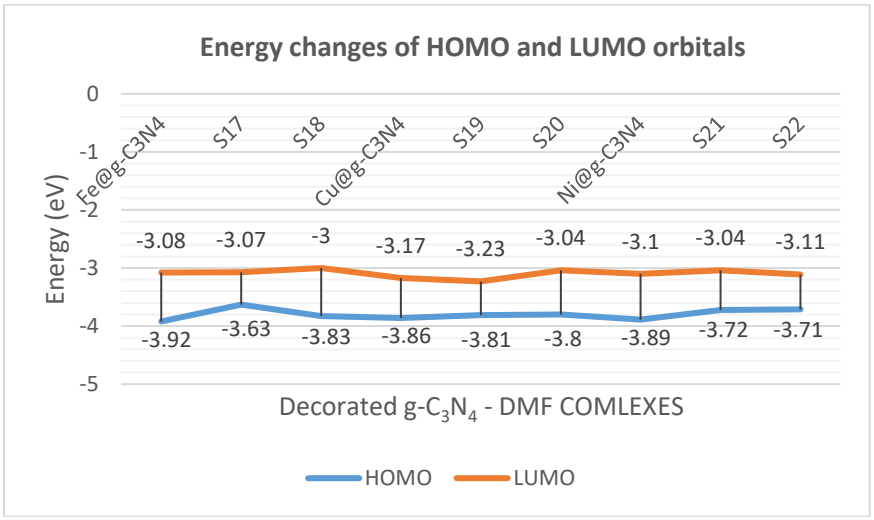

Fig. 8. The variations in HOMO and LUMO energy levels within complexes S17 to S22.

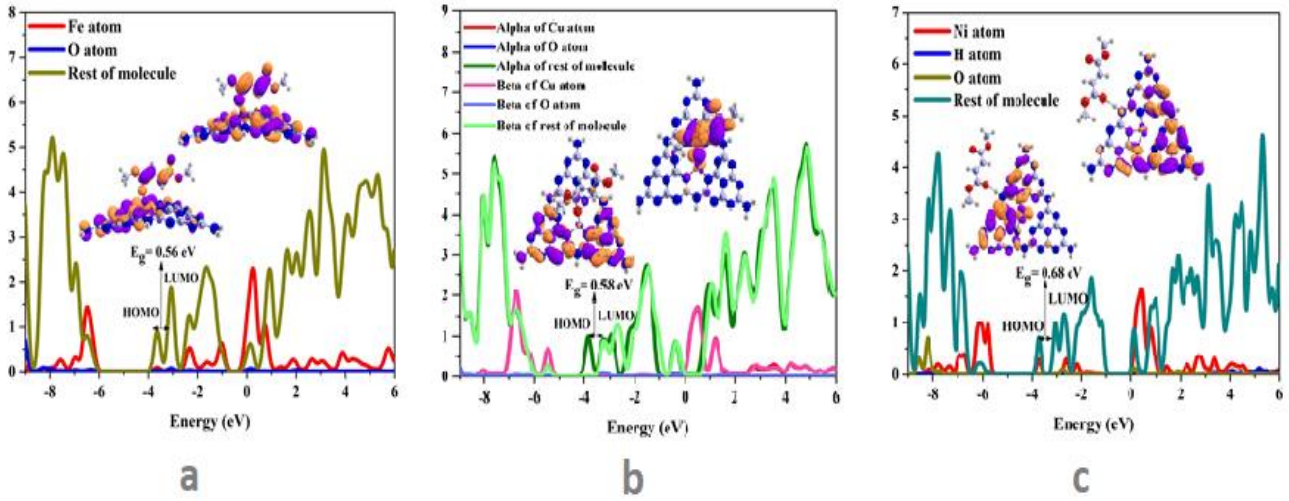

Fig. 9. PDOS plots of the decorated g-C_3N_4 with (a) Fe atom (Fe@ g-C_3N_4), S17 configuration, (b) Cu atom (Cu@ g-C_3N_4), S19 configuration (c) Ni atom (Ni@ g-C_3N_4), S21 configuration in the gas phase.

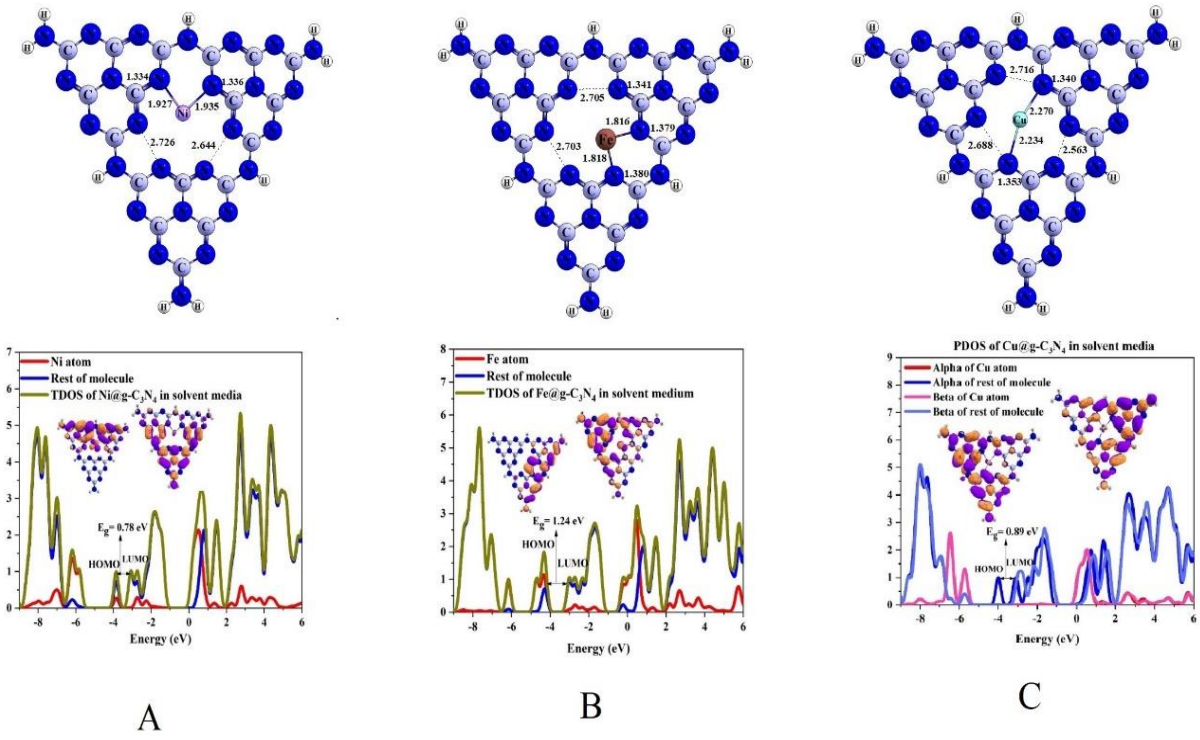

Fig. 10. Optimized structures and PDOS plots of the decorated g-C_3N_4 with of (A) Ni@ g-C_3N_4 (B) Fe@g-C_3N_4 (C) Cu@g-C_3N_4 in solvent phase.

The comparative analysis of the gap energies for these six structures is as follows:

S23 > S24 > S26 > S25 > S28 > S27

A reduction in the gap energy of the complex results in a negative change in gap energy (%ΔEg), which correlates with an enhanced capacity for electrical signal conduction, thereby indicating improved conditions for sensor functionality. The most significant change in the energy gap is observed in the S25 structure, exhibiting a value of -13.48%. The variations in gap energy suggest that structures S24, S25, and S27 may serve as promising candidates for a dimethyl fumarate drug sensor.

The positive value of the charge transfer factor (QT) indicates that electric charge is being transferred from the surface of the decorated g-C_3N_4 to the surface of the DMF. Notably, in the S23 structure, a charge transfer occurs

from the drug to the Fe@g-C_3N_4, resulting in a remarkable negative value of -619. In contrast, the other structures exhibit positive charge transfer values. Among these, the S25 structure demonstrates the highest charge transfer from the decorated g-C_3N_4 surface to dimethyl fumarate, chemical adsorption interaction. Conversely, the adsorption energies for structures S24 and S25 indicate a favorable physical adsorption process. The selection of sensors and drug carriers is significantly influenced by adsorption energy and gap energy. Among the Fe@g-

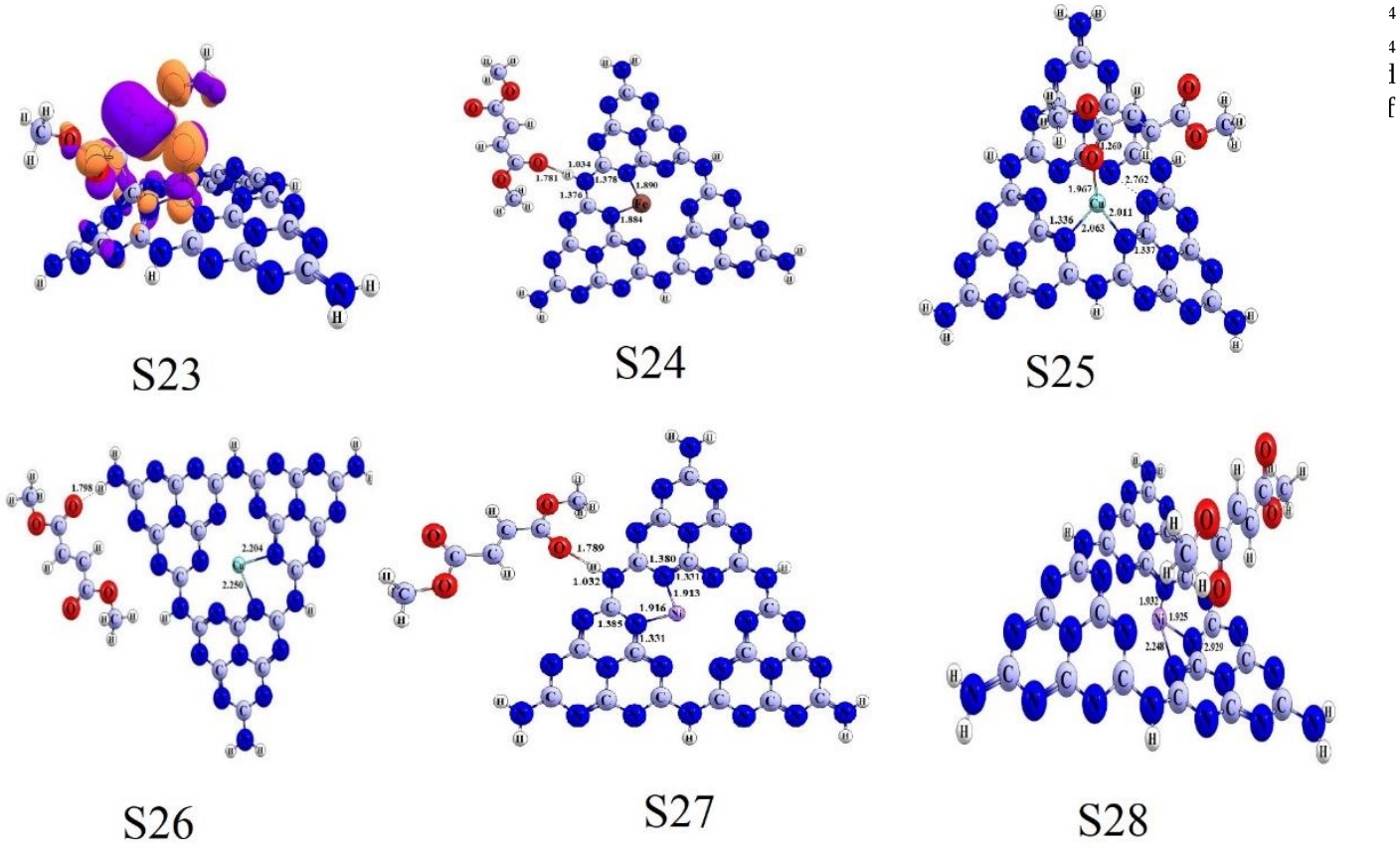

Fig. 11. Optimized structures of DMF- decorated g-C_3N_4 complexes in solvent phase. Distances are in A.

Table 8- Adsorption energy (Eads), Energy of HOMO and LUMO orbitals, energy difference of HOMO and LUMO orbitals (Eg), Fermi level energy (EFL), the change of energy gap of g-C_3N_4 after adsorption (%ΔEg), work function (Φ), the change of work function of g-C_3N_4 after adsorption (ΔΦ), and Charge transfer between DMF molecule and decorated g-C_3N_4 (QT) in the solvent phase.

Systems	E_{ads} (kcal/mol)	E_{HOMO} (eV)	E_{FL} (eV)	E_{LUMO} (eV)	E_g (eV)	$\%\Delta E_g$	Φ (eV)	ΔΦ (eV)	Q_T (me)
Fe@g-C_3N_4	**-**	**-4.25**	**-3.63**	**-3.01**	**1.24**	**-**	**3.63**	**-**	**-**
S23	**-57.59**	**-5.18**	**-4.16**	**-3.14**	**2.04**	**64.52**	**4.16**	**0.53**	**-619**
S24	**-10.77**	**-4.14**	**-3.59**	**-3.05**	**1.09**	**-12.10**	**3.59**	**-0.04**	**29**
Cu@g-C_3N_4	**-**	**-3.98**	**-3.53**	**-3.09**	**0.89**	**-**	**3.53**	**-**	**-**
S25	**-14.20**	**-3.98**	**-3.59**	**-3.21**	**0.77**	**-13.48**	**3.59**	**0.06**	**81**
S26	**-5.84**	**-3.96**	**-3.51**	**-3.06**	**0.90**	**1.12**	**3.51**	**-0.02**	**27**
Ni@g-C_3N_4	**-**	**-3.85**	**-3.46**	**-3.07**	**0.78**	**-**	**3.46**	**-**	**-**
S27	**-6.10**	**-3.79**	**-3.42**	**-3.06**	**0.73**	**-6.41**	**3.42**	**-0.04**	**26**
S28	**-3.69**	**-3.82**	**-3.44**	**-3.06**	**0.76**	**-2.56**	**3.44**	**-0.02**	**7**

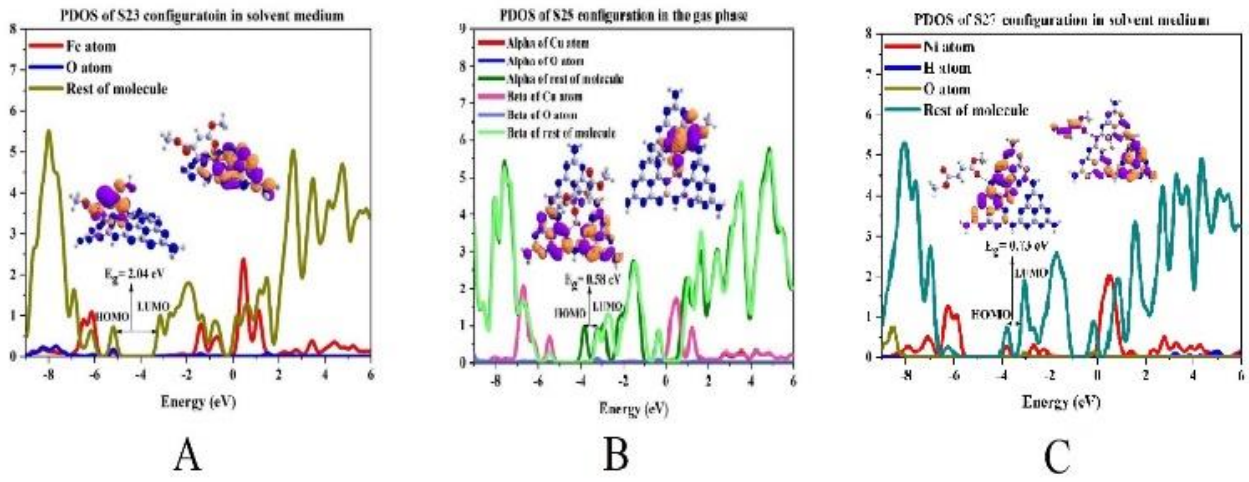

Fig. 12. PDOS plots of the decorated g-C_3N_4 with (a) Fe atom (Fe@ g-C_3N_4), S23 configuration, (b) Cu atom (Cu@ g-C_3N_4), S25 configuration (c) Ni atom (Ni@ g-C_3N_4), S27 configuration in the solvent phase.

4. Conclusion

In this research, the sensing ability and the energy of interactions between Dimethyl Fumarate (DMF) and the pristine, Fe, Cu and Ni-decorated graphitic carbonitride (g-C_3N_4) has been studied by using density functional theory (DFT) calculations. Also, the adsorption behavior of pristine g-C_3N_4, Fe- and Cu- and Ni-decorated g-C_3N_4 has been investigated toward DMF. Within the context of pristine g-C_3N_4-DMF complexes in the gas phase, the S1 structure emerges as the most promising candidate for sensor applications. This is evidenced by its adsorption energy, which is recorded at -10.86 Kcal.mol^{-1}, alongside a notable change in the energy gap of -3.86. *These* parameters indicate that the S1 structure exhibits superior characteristics compared to other g-C_3N_4-DMF complexes under gaseous conditions. In the context of g-C_3N_4-DMF complexes within the aqueous phase, no appropriate candidate emerged for sensor application. These structures designated as S9 exhibited the most significant adsorption energy, quantified at -6.59 Kcal.mol^{-1}, suggesting a favorable physical adsorption process that necessitates minimal inhibition time. However, it is noteworthy that the energy gap for this particular complex remained unchanged and the change of the energy gap recorded at zero. Conversely, other complexes under similar conditions demonstrated the change of the energy gap of less than 1. In the gaseous phase, the Ni@ g-C_3N_4- DMF complexes exhibit promising characteristics, particularly in structures S21 and S22, which demonstrate adsorption energies of -10.24 and -7.42 Kcal.mol^{-1}, respectively. These negative values suggest effective physical adsorption. Furthermore, the change of the energy gap for these complexes are recorded at -13.92 and -24.05, indicating a notable sensitivity of Ni@g-C_3N_4 to DMF presence and the application of a sensor. In the solvent phase, structure S27 reveals that Ni@g-C_3N_4 can function as a sensor for DMF, with an adsorption energy of -6.10 Kcal.mol^{-1} and the change of the energy gap -6.41, further supporting its potential utility in sensing applications. Among the complexes formed between Fe@ g-C_3N_4 and DMF, two notable structures, S17 and S24, have been examined in both gas and solvent phases, respectively. The energy gap changes for these complexes are recorded at -33.33 and -12.10, while their corresponding adsorption energies are -18.32 and -10.77 Kcal.mol^{-1}. These findings suggest that Fe@g-C_3N_4 demonstrates potential as an effective sensor for DMF in both gaseous and solvent phases. In contrast, complex S23, which pertains to the solvent phase, exhibited the highest adsorption energy in this study, measured at -57.59 Kcal.mol^{-1}. This significant value indicates a very strong chemical adsorption, rendering it unsuitable for applications as a sensor or drug carrier. The investigation of the complexes formed between Cu@ g-C_3N_4 and DMF has revealed two significant structures, designated as S19 and S25, which have been analyzed in gas and solvent phases, respectively. The observed variations in energy gaps for these complexes are -15.94 and -13.48, respectively, while their associated adsorption energies are recorded at -7.67 and -14.20 Kcal.mol^{-1}. These results indicate that Cu@ g-C_3N_4 may serve as a promising sensor for DMF across both gaseous and liquid phases.

References

[1] A. Thomas, A. Fischer, F. Goettmann, M. Antonietti, J.-O. Müller, R. Schlögl, J.M. Carlsson, Graphitic carbon nitride materials: variation of structure and morphology and their use as metal-free catalysts. *J. Mater. Chem*. (2008): 18 (41) 4893–4908.

[2] D.M. Teter, R.J. Hemley, Low-compressibility carbon nitrides. *J. Science* (1996): 271 (5245) 53–55.

[3] S. Ahmadi, A. Hosseinian, P. Delir Kheirollahi Nezhad, A. Monfared, E. Vessally. Nano-Ceria (CeO2): An Efficient Catalyst for the Multi-Component Synthesis of a Variety of Key Medicinal Heterocyclic Compounds. *Iran. J. Chem. Chem. Eng. (IJCCE)* (2019): 38(6): 1-19.

[4] A. Tariq, S. Nazir, A. Wahab Arshad, J. Iqbal. DFT study of the therapeutic potential of phosphorene as a new drug-delivery system to treat cancer. *RSC Advances* (2019): 9, 24325.

[5] B. Azizi, M.R.P Heravi, Z. Hossaini, A. Ebadi, E. Vessally, Intermolecular Difunctionalization of Alkenes: Synthesis of B-Hydroxy Sulfides. *RSC Adv* (2021): 11: 13138-13151.

[6] E. Babanezhad, A. Beheshti. The Possibility of Selective Sensing of the Straight-Chain Alcohols (Including Methanol to n-pentanol) by Using the C20 Fullerene and C18NB Nano Cage. *Chem. Rev. Lett* (2018): 1:82–88.

[7] W. Baran, E. Adamek, J. Ziemia-Nska, A. Sobczak, Effects of The Presence of Sulfonamides in the Environment and Their Influence on Human Health. *J. Hazard. Mater* (2011): 196: 1-15.

[8] R.H. Baughman, A.A. Zakhidov, W.A. De Heer, Carbon Nanotubes--the Route Toward Applications. *J. Science* (2002): 297: 787-792.

[9] J. Beheshtian, A.A. Peyghan, Z. Bagheri, Detection of Phosgene by Sc-Doped BN Nanotubes: A DFT Study. *Sens. Actuators B. Chem* (2012): 171:846–852.

[10] F. Behmagham, Z. Asadi, Y. Jamal Sadeghi, Synthesis, Spectroscopic and Computational Investigation of Bis (3-methoxyphenylthio) ethyl) Naphthalene. *Chem. Rev. Lett* (2018): 1:68–76.

[11] A.S. Berdinsky, Y.V. Shevtsov, A.V. Okotrub, S.V. Trubin, L.T. Chadderton, Sensor Properties of Fullerene Films and Fullerene Compounds with Iodine. *Chemistry for Sustainable Development* (2000): 8: 141-146.

[12] A. Białk- Bielinska, S. Stolte, J. Arning, U. Uebers, A. Boschen, P. Stepnowski, M. Matzke, Ecotoxicity Evaluation of Selected Sulfonamides, *Chemosphere* (2011): 85(6): 928–933.

[13] S.F. Boys, F. Bernardi, The Calculation of Small Molecular Interactions by Differences of Separate Total Energies - Some Procedures with Reduced Errors. *J. Molecul. Physics*, (1970): 19(4): 553-561.

[14] H. Chou-Yi, H. Riyadh Abdul Kareem Al-Hett. A DFT study on the probability of using the heteroatom decorated graphitic carbonitride (g-C3N4) species for delivering of three novel Multiple sclerosis drugs. *Molecular Graphics and Modelling* (2023): 125 - 108605.

[15] (a) E. Vessally, S. Soleimani-Amiri, A. Hosseinian, L. Edjlali, A. Bekhradnia, The Hartree-Fock exchange effect on the CO adsorption by the boron nitride nanocage, *Physica E Low Dimens. Syst. Nanostruct*., 87 (2017) 308-311; (b) A. Hosseinian, S. Soleimani-amiri, S. Arshadi, E. Vessally, L. Edjlali, Boosting the adsorption performance of BN nanosheet as an anode of Na-ion batteries: DFT studies, *Phys. Lett. A*, 381 (2017) 2010-2015; (c) S. Esfahani, J. Akbari, S. Soleimani-Amiri, Adsorption of Ibuprofen by an Iron-doped Silicon Carbide Graphene monolayer: DFT exploration of drug delivery insights, *Int. J. Nano Dimens.*, 15 (2024) 63-71; (d) A.S. Hessen, N.M. Ahmed Alsultany, H. Bahir, A.H. Adthab, S. Soleimani-Amiri, S. Ahmadi, E. Vessally, A. Khanmohammadi, Adsorption of sulfur mustard on the transition metals (TM = Ti^{2+}, Cr^{2+}, Fe^{2+}, Co^{2+}, Ni^{2+}, Cu^{2+}, Zn^{2+}) porphyrins induced in carbon nanocone (TM-PCNC): Insight from DFT calculation, *J. Mol. Graphics Modell*., 135 (2025) 108928.

[16] (a) D.R. Dietrich, S.F. Webb, T. Petry, Hot Spot Pollutants: Pharmaceuticals in the Environment. *Toxicology Letters* (2002): 131(1-2): 1-3; (b) S. Esfahani, J. Akbari, S. Soleimani-Amiri, M. Mirzaei, A.G. Gol, Assessing the drug delivery of ibuprofen by the assistance of metal-doped graphenes: insights from density functional theory, *Diam. Relat. Mater.*, 135 (2023) 109893; (c) M.R. Poor Heravi, B. Azizi, E. Abdulkareem Mahmood, A.G. Ebadi, M.J. Ansari, S. Soleimani-Amiri, Molecular simulation of the paracetamol drug interaction with Pt-decorated BC3 graphene-like nanosheet, *Mol. Simul.*, 48 (2022) 517-525.

[17] (a) HA. Blair. "Dimethyl Fumarate: A Review in Relapsing-Remitting MS. Drugs (2019): 1965-1976. doi: 10.1007/s40265-019-01229-3. PMID: 31784875; (b) M. Afshar, R. Ranjineh Khojasteh, R. Ahmadi, M. Nakhaei Moghaddam, In silico adsorption of lomustin anticancer drug on the surface of boron nitride nanotube, *J. Chem. Lett.*, 4(3) (2021) 178-184; (c) A. Karbakhshzadeh, S. Majedi, V. Abbasi, Computational investigation on interaction between graphene nanostructure BC3 and Rimantadine drug: Possible sensing study of BC3 and its doped derivatives on Rimantadine, *J. Chem. Lett.*, 3 (2022) 108-113; (d) B. Mohammadi, M. R. Jalali Sarvestani, A Comparative Computational Investigation on Amantadine Adsorption on the Surfaces of Pristine, C-, Si-, and Ga-doped Aluminum Nitride Nanosheets, *J. Chem. Lett.* 4 (2023) 66-70.

[18] (a) A. Hassanpour, M. R. P. Heravi, A. Ebadi, Hosseinian A., E. Vessally ,Oxidative Trifluoromethyl (thiol/selenol) ation of Terminal Alkynes: An Overview. *Journal of Fluorine Chemistry* (2021): 109-762; (b) B. Ajdari, S. A. Vahed, Fullerene (C20) as a sensing material for electrochemical detection of Nortriptyline: A theoretical study, *J. Chem. Lett.*, 3 (2022) 164-168; (c) M. Jalali Sarvestani, Venlafaxine Interaction with Fullerene (C20): DFT Studies, J. Chem. Lett. 3 (2022) 169-173.

[19] M. R.P Heravi, S.Habibzadeh, A. G. Ebadi, P.D. Kheirollahi Nezhad, E. Vessally, Substituent Effects of Fused Hammick Silylenes via Density Functional Theory Survey." *Phys. Org. Chem* (2021): 34(11): 4264 .

[20] M.R.P Heravi, A. Hosseinian, Z. Rahmani, A. Ebadi, E. Vessally, Transition- Metal- Catalyzed Dehydrogenative

Coupling of Alcohols and Amines: a Novel and Atom-Economical Access to Amides ." *J. Chin. Chem. Soc* (2021): 68(5): 723-737.

[21] J. Howard, S. Trevick, Epidemiology of multiple sclerosis. *Neurol Clin* (2016): 34:919-39.

[22] M. Jalali Sarvestani, N. Mert, E. Vessally, "Cross Dehydrogenative Coupling of Aldehydes with NHydroxyimides: An Efficient and Straightforward Route to N-Hydroxyimides Esters." *J. Chem. Lett* (2020): 1(3): 93-102.

[23] J. Jia, Y. Cao, T. Wu, Y. Tao, Pan Y., Huang F., Tang H. "Highly Regio- and Stereoselective Markovnikov Hydrosilylation of Alkynes Catalyzed by High-Nuclearity {Co14} Clusters." *ACS Catalysis* (2021): 11(12): 6944-6950.

[24] O.A.H. Jones, N. Voulvoulis, J.N. Lester "Human Pharmaceuticals in the Aquatic Environment*." A Review, Environ. Technol* (2001): 22(12): 1383-1394 .

[25] K. Kummerer, Ed. Springer "A Data Based Perspective on the Environmental Risk Assessment of Human Pharmaceuticals II Aquatic Risk Characterization." *Pharmaceuticals in the Environment: Sources, Fate, Effects and Risks.* 2001. 203-19.

[26] R.T. Kareem, B. Azizi, M. Asnaashariisfahani, A. Ebadi, E. Vessally "Vicinal Halo-Trifluoromethylation of Alkenes*." RSC Advances* (2021): 11(25): 14941-14955 .

[27] H. Liu, Y. Wang, Q. Li, N. Yang, Z. Wang, Q. Wang "Research on the Evolution Characteristics of Oxygen-Containing Functional Groups During the Combustion Process of the Torrefied Corn Stalk." *Biomass and Bioenergy* (2022): 158.

[28] Z. Liu, A. Ebadi, M. Toughani, N. Mert N, E. Vessally "Direct Sulfonamidation of (Hetero)Aromatic C–H Bonds with Sulfonyl Azides: A Novel and Efficient Route to N-(Hetero)Aryl Sulfonamides." *RSC. Adv* (2021): 10: 37299-37313.

[29] M.H Sayadi. Contamination of Soil in Industrial Area. Lambert. Academic. Publishing, Germany, 2010.

[30] Z. Kexin, W. Yonggang, A.G. Ebadi, M. Toughani. "Investigation of Low-Temperature Lipase Production and Enzymatic Properties of Aspergillus Niger." *Iran. J. Chem. Chem. Eng. (IJCCE)* (2021): 49(4): 1364-1374.

[31] M. Perveen, A. Tariq, S. Nazir, A. Wahab Arshad, J. Iqbal. "Therapeutic potential of graphitic carbon nitride as a drug delivery system for cisplatin (anticancer drug): A DFT approach." *Biophysical Chemistry* (2022): 267-106461.

[32] M.Perveena, S.Nazirb, A.Wahab, M. Issa Khan, M. Shamim,J. Iqbal. " DFT study of therapeutic potential of graphitic carbon nitride (g-C3N4) as a new drug delivery system for carboplatin to treat cancer." *Journal of Molecular Liquids* (2021): 331-115607.

[33] S. Mohammadi, M. Musavi, F. Abdollahzadeh, SH. Babadoust, A. Hosseinian "Application of NanoCatalysts in C-Te Cross-coupling Reactions: An Overview." *Chem. Rev. Lett* (2018): 1: 49–55.

[34] S. Mu, Q. Liu, P. Kidkhunthod, X. Zhou, "Molecular Grafting Towards High-Fraction Active Nanodots Implanted in N-Doped Carbon for Sodium Dual-Ion Batteries." *National Science Review* (2020): 8(7).

[35] V. Nagarajan, R. Chandiramouli "TeO2 Nano Structures as a NO2 Sensor: DFT Investigation." *Comput. Theorei. Chem* (2014): 1049: 20-27.

[36] K. Noyes, B. Weinstock-Guttman "Impact of diagnosis and early treatment on the course of multiple sclerosis." *Am J Manag Care* (2013 Nov): 19(17 Suppl):s321-31.

[37] N. OBoyle, A. Tenderholt, K. Langner "A Library for Package Independent Computational Chemistry Algorithms." *J. Comput. Chem* (2008): 29(5): 839-845.

[38] H. Kitahara, L. Narita " Formation Atomic Structures and Properties of Boron Nitride and Carbon Nanocage Fullerene Materials." *International. J. Inorgan. Mater* (2001): 3(7): 597-612.

[39] M. Petrovic, S.Gonzalez, D. Barcelo "Analysis and Removal of Emerging Contaminants in Waste Water and Drinking Water." *Trends. Anal. Chem* (2003): 22(10): 685–696.

[40] A.A. Peyghan, M. Moradi "First-Principle Study of Methanol Adsorption on Ni(Pd)-Decorated Graphene ." *J. Iran. Chem. Soc* (2015): 12: 751-756.

[41] E. Pop , D. Mann, Q. Wang, K. Goodson, H. Dai, "Thermal Conductance of an Individual Single-Wall Carbon Nanotube Above Room Temperature." *Nano. Lett.* (2006): 6: 96-100.

[42] R.G, Parr. Density Functional Theory of Atoms and Molecules. *International Academy of Quantum Molecular Science*, 1980.

[43] (a) N. E. B.Saidu, K. Leroy, C. Jacob, "Dimethyl fumarate, a two-edged drug: Current status and future directions." *Medicinal Research Reviews* (2019): 10.1002/med.21567; (b) F.N.U. Srinidhi, Artificial Neural Network (FFBP-ANN) Based Grey Relational Analysis for Modeling Dyestuff Solubility in Supercritical CO_2 with Ethanol as the Co-Solvent, *Chem. Rev. Lett.* 6 (2022) 141-152.

[44] (a) M. Samadizadeh, S.F. Rastegar, A.A. Peyghan "F−, Cl−, Li+ and Na+ Adsorption on AlN Nanotube Surface: a DFT Study." *Physica. E* (2015): 69:75–80; b) B. Mirza, S. Soleimani-Amiri, M. Mirza, Reaching for [6]n SiC-cyclacenes and [6]n SiC-acenes: A DFT approach, *J. Phys. Org. Chem.*, 31 (2018) e3754; (c) S. Soleimani Amiri, M. Koohi, B. Mirza, Characterizations of B and N heteroatoms as substitutional doping on structure, stability, and aromaticity of novel heterofullerenes evolved from the smallest fullerene cage C20: a density functional theory perspective, *J. Phys. Org. Chem.*, 29 (2016) 514-522; (d) M.Z. Kassaee, F. Buazar, S. Soleimani-Amiri, Triplet germylenes with separable minima at ab initio and DFT levels, *J. Mol. Struct. THEOCHEM*, 866 (2008) 52–57.

[45] (a) M.H. Sayadi, R.K. Trivedy, R.K. Pathak "Pollution of Pharmaceutical in Environment." *J. Industr. Pollut. Control*, (2010): 26(1): 89-94; (b) S. Soleimani-Amiri, Identification of Structural, Spectroscopic, and Electronic Analysis of Synthesized 4-(5-Phenyl-1, 3, 4-Oxadiazol-2-Ylthio)-3-Methylbenzene-1, 2-Diol: A Theoretical Approach, *Polycyclic Aromat. Compd.*, 41 (2021) 635-

652. (c) S. Soleimani-Amiri, Singlet and triplet cyclononа-3,5,7-trienylidenes and their α, ά-halogenated derivatives at DFT, *J. Phys. Org. Chem.*, 33 (2020) e4018; (c) S. Soleimani-Amiri, S. Badragheh, N. Asadbeigi, A theoretical study of electronic effects in alkyne-linked reactive intermediates: (nitrenoethynyl)methylenes,(nitrenoethynyl)silylenes, and (nitrenoethynyl)germylenes, *J. Chin. Chem. Soc.*, 66 (2019) 866-880.

[46] (a) C. Shi , Z. Wu , F. Yang , Y. Tang. "Particles with pH Switchable Properties for High-Efficiency Adsorption of Ppcps in Water." *Solid State Sciences* (2021): 119: 106702; (b) B. Hashemzadeh, L. Edjlali, P. Delir Kheirollahi Nezhad, E. Vessally, A DFT studies on a potential anode compound for Li-ion batteries: Hexa-cata-hexabenzocoronene nanographen, *J. Chem. Lett.* 4(4) (2021) 232-238; (c) N. Salehi, E. Vessally, l. Edjlali, I. Alkorta, M. Eshaghi, Nan@ Tetracyanoethylene (n= 1-4) systems: Sodium salt vs Sodium electride, *Chem Rev Lett*., 3 (2020) 207-217; (d) M. Kamel, K. Mohammadifard, Thermodynamic and reactivity descriptors Studies on the interaction of Flutamide anticancer drug with nucleobases: A computational view, *Chem. Rev. Lett.* 4(1) (2021) 54-65.

[47] (a) S. Soleimani-Amiri, N. Asadbeigi, S. Badragheh " A Theoretical Approach to New Triplet and Quintet (nitrenoethynyl) alkylmethylenes,(nitrenoethynyl) alkylsilylenes,(nitrenoethynyl) alkylgermylenes." *Iran. J. Chem. Chem. Eng. (IJCCE)* (2020): 39(4): 39-52; (b) S. Esfahani, J. Akbari, S. Soleimani-Amiri, Novel ionic liquid systems based on three-nitro phenoxide: Spectroscopic and electronic characterization using theoretical and experimental study, *Main Group Chem.*, 23 (2024) 283-297; (c) M.M. Kadhim, E.A. Mahmood, V. Abbasi, M.R. Poor Heravi, S. Habibzadeh, S. Mohammadi-Aghdam, S. Soleimani-Amiri, Investigation of the substituted—titanium nanocages using computational chemistry, *J. Mol. Graphics Modell.*, 118 (2023) 108317.

[48] C. Tabtimsai, V. Ruangpornvisuti, B.Wanno, "Density Functional Theory Investigation of the VIIIB Transition Metal Atoms Deposited on (5, 5) Single Walled Carbon Nanotubes." *Physica. E* (2013): 49: 61-67.

[49] E. Vessally, S. Mohammadi, M. Abdoli, A. Hosseinian, P. Ojaghloo, "Convenient and Robust Metal-Free Synthesis of Benzazole-2-Ones Through the Reaction of Aniline Derivatives and Sodium Cyanate in Aqueous Medium" *Iran, J. Chem. Chem. Eng. (IJCCE) (*2020): 39(5): 11.

[50] E. Vessally, M.R Poor Heravi. "A Density Functional Theory Study of Adsorption Ethionamide on the Surface of the Pristine, Si and Ga and Al-Doped Graphene." *Iranian Journal of Chemistry and Chemical Engineering* (2021): Article Vol. 40, No. 6, 1720.

[51] M. Wang, C. Jiang, S. Zhang, X. Song, Y. Tang, H. Cheng "Reversible Calcium Alloying Enables a Practical Room-Temperature Rechargeable Calcium-Ion Battery with a High Discharge Voltage." *Nature chemistry* (2018): 10(6): 667-672.

[52] W. Xu, A.G. Ebadi, M. Toughani, E. Vessally "Incorporation of CO2 into Organosilicon Compounds via Csi Bond Cleavage." *Journal of CO2 Utilization* (2020): 101358.

[53] Y. Kang, Y. Yang , L. Yin , X. Kang , G. Liu. "An Amorphous Carbon Nitride Photocatalyst with Greatly Extended Visible-Light-Responsive Range for Photocatalytic Hydrogen Generation." *Adv. Mater.* (2015): 27, 4572–4.

[54] M. Zhang , X. Sun, C. Wang, Y. Wang, Z. Tan, "Photocatalytic Degradation of Rhodamine B Using Bi4O5Br2-doped ZSM-5." *Materials chemistry and physics* (2022): 278: 125697 .

[55] X. Zhang , Y.Tang, F. Zhang , "A Novel Aluminum-Graphite Dual-Ion Battery." *Advanced Energy Materials* (2016): 6(11): 1502588.

[56] Y. Zheng, et al. "Graphitic Carbon Nitride Polymers toward Sustainable Photoredox Catalysis." *Angew. Chem* (2015): 54, 12868−12884.

[57] W. Zhou, J. Zhou, J. Shen, C. Ouyang, S. Shi "First Principles Study of High-Capacity Hydrogen Storage on Graphene with Li Atoms." *J. Physics. Chem. Solids* (2012): 73(2): 245-251.

[58] E. Zuccato, D. Calamari, M. Natangelo, R. Fanelli "Presence of Therapeutic Drugs in the Environment." *Lancet* (2000): 355(9217): 1789-90.